Functional Mesoporous Carbon-Coated Separator for Long-Life, High-Energy Lithium–Sulfur Batteries

Juan Balach, Tony Jaumann, Markus Klose, Steffen Oswald, Jürgen Eckert, and Lars Giebeler*

The lithium–sulfur (Li–S) battery is regarded as the most promising rechargeable energy storage technology for the increasing applications of clean energy transportation systems due to its remarkable high theoretical energy density of 2.6 kWh kg^{-1}, considerably outperforming today's lithium-ion batteries. Additionally, the use of sulfur as active cathode material has the advantages of being inexpensive, environmentally benign, and naturally abundant. However, the insulating nature of sulfur, the fast capacity fading, and the short lifespan of Li–S batteries have been hampered their commercialization. In this paper, a functional mesoporous carbon-coated separator is presented for improving the overall performance of Li–S batteries. A straightforward coating modification of the commercial polypropylene separator allows the integration of a conductive mesoporous carbon layer which offers a physical place to localize dissolved polysulfide intermediates and retain them as active material within the cathode side. Despite the use of a simple sulfur–carbon black mixture as cathode, the Li–S cell with a mesoporous carbon-coated separator offers outstanding performance with an initial capacity of 1378 mAh g^{-1} at 0.2 C, and high reversible capacity of 723 mAh g^{-1}, and degradation rate of only 0.081% per cycle, after 500 cycles at 0.5 C.

1. Introduction

The overwhelming advances in lithium-battery technology have had a far-reaching impact on today's life. This influence has not only revolutionized the market of small electric portable devices but also propelled the development of current hybrid electric vehicles (HEVs). However, the state-of-the-art lithium-ion (Li-ion) batteries, which commonly contain high-voltage intercalation cathodes (i.e., $LiCoO_2$, $LiFePO_4$, and $LiNiMnCoO_2$) with theoretical capacities of less than 300 mAh g^{-1}, are not capable to meet the specific energy requirements for future all-electric vehicles (EVs) and grid-scale energy storage applications.[1] To address the energy demands of tomorrow, development and implementation of new energy storage alternatives are highly required. In this regard, the lithium–sulfur (Li–S) battery is one of the most interesting potential candidates for next-generation rechargeable batteries since pure sulfur as cathode material exhibits a high theoretical specific capacity of 1672 mAh g^{-1} and, despite the lowered discharge potential compared to intercalation electrodes, the Li/S coupling can deliver a high energy density of 2600 Wh kg^{-1} (based on the complete reaction of sulfur with lithium to form Li_2S) which is up to five times higher than current Li-ion batteries.[2] In addition, sulfur has the favorable advantages of being inexpensive, environmentally benign and naturally abundant in almost infinite quantities.

However, the fast capacity fading and the short lifespan of Li–S batteries have so far hampered their commercial application. While the insulating nature of sulfur limits its electrochemical activity, the poor cyclability and the low Coulombic efficiency (CE) are mainly due to the loss of active material by the shuttle of dissolved lithium polysulfide (LiPS) intermediates (Li_2S_n, $4 < n \leq 8$) between the anode and the cathode.[3] So far, several strategies have been proposed in order to tackle these issues and improve the overall electrochemical performance of the Li–S batteries.[4] Among them, the preparation of sulfur–carbon composites by confining sulfur into the cavity of some hollow or porous carbon hosts, allowing intimate contact between the active material and the conductive matrix is the frequently used approach.[5] The protection of the lithium anode by using additives or conductive polymers has also shown a favorable advance on the performance of Li–S batteries.[6] Addressing the safety problems of Li metal anodes, there is an increasing interest to find safe substitutes, actually favoring prelithiated tin or silicon anodes and Li_2S cathodes.[7]

Recently, the reconfiguration of the Li–S cell has been proposed. This approach involves the insertion of a freestanding carbon interlayer between the separator and the sulfur cathode to both reduce internal resistance of the cells and trap soluble LiPS intermediates.[8] In this regard, we demonstrated that the pore volume of mesoporous carbon interlayers plays an important role on the cycling performance of Li–S batteries.[8e]

Dr. J. Balach, T. Jaumann, M. Klose, Dr. S. Oswald, Prof. J. Eckert, Dr. L. Giebeler
Institute for Complex Materials
Leibniz Institute for Solid State and Materials Research (IFW) Dresden
Helmholtzstraße 20, D-01069 Dresden, Germany
E-mail: j.balach@ifw-dresden.de
Prof. J. Eckert, Dr. L. Giebeler
Institut für Werkstoffwissenschaft
Technische Universität Dresden
Helmholtzstraße 7, D-01069 Dresden, Germany

DOI: 10.1002/adfm.201502251

© 2015 WILEY-VCH Verlag GmbH & Co. KGaA, Weinheim

Following a similar in situ polysulfide-trapping concept, carbon nanotubes- and microporous carbon-coated separators have been recently reported.[9] Such designed separators integrate the functionalities shown for freestanding carbon interlayers and also decrease the weight and thickness of the carbon layer, resulting in a higher specific energy density. To the best of our knowledge, the modification of the commercially used separator with mesoporous carbons has not been reported so far. From a practical application point of view, modified separators with a thin layer of mesoporous carbon represent a highly interesting pathway to amplify the separator functions and improve the electrochemical performance of Li–S batteries. Compared with our previous mesoporous carbon interlayer used in a cell configuration composed of four main components (anode, separator, carbon interlayer, and cathode),[8e] the use of the current hybrid carbon/polypropylene separator not only decreases the weight and thickness of the coating layer but also allows a cell setup with three main components commonly used in battery manufacturing, simplifying the assembly process of the cells by the elimination of one of the components. The simple processing technique for the fabrication of our modified separator accompanied by the remarkable improvement of the electrochemical performance of the Li–S cells is a practically focused solution which can be easily transferred into industrial processes. Furthermore, we highlight that high capacities and long cycle life can be obtained through a straightforward ball-milled sulfur–carbon black mixture without the need to implement long melt-infiltration procedures typically used to incorporate sulfur into porous carbon hosts.

In this paper, we present a mesoporous carbon-coated (mesoC-coated) separator for suppressing the migration of soluble LiPSs which thus enhances the overall electrochemical performance of Li–S batteries despite the use of a simple pure sulfur–carbon black mixture as cathode. For the modification of the porous polypropylene separator (Celgard separator), a light-weight mesoporous carbon (mesoC) with large pore volume was prepared by polymerization of resorcinol with formaldehyde in the presence of colloidal silica nanoparticles (12 nm in diameter) and its subsequent carbonization and silica template removal. A schematic configuration of the Li–S cells with pristine separator and mesoC-coated separator is shown in **Scheme 1**. In general, a battery separator prevents physical contact and, thus, a short circuit between anode and cathode, while allowing ion transport in the cell. However, this last required property also facilitates the undesired migration of dissolved LiPS products generated during the discharge–charge cycles (Scheme 1a), causing further contamination of the lithium anode and the self-discharge of the cell through a polysulfide shuttle mechanism.[9e] While our modified separator keeps its primary functions, the features of the thin mesoC coating (covering the side of the separator facing the cathode), acts as a second current collector to increase the electrical conductivity of the cell,[8a] and serves as a physically intrinsic mesoporous framework reservoir for the early trapping and confinement of dissolved LiPSs. Additionally, the mesoscale void-space of the mesoC is able to accommodate the large volume change of sulfur during lithiation (Scheme 1b). Compared with the pristine separator, the use of the mesoC-coated separator as LiPS barrier can reduce the shuttle effect and improves the active material utilization, which consequently enhances the electrochemical performance and prolongs the cycle life of Li–S batteries.

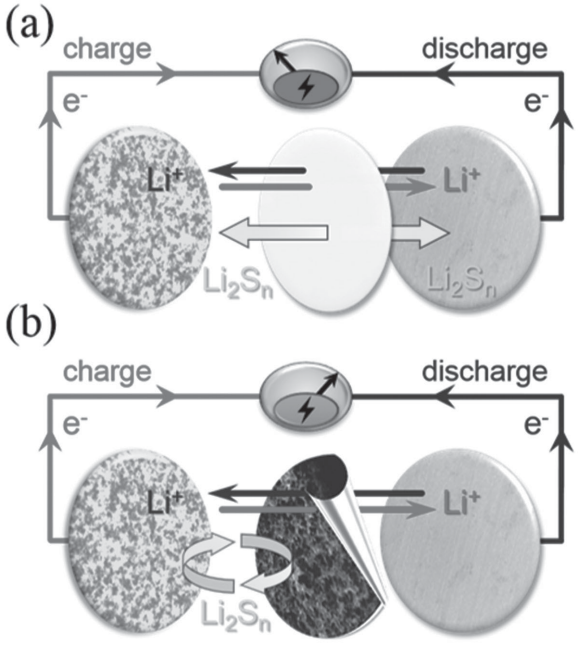

Scheme 1. Schematic configuration of the Li–S cells with a) pristine separator and b) mesoC-coated separator. The cell configuration is composed of, from left to right, a sulfur cathode, the corresponding separator, and a lithium anode.

2. Results and Discussion

The textural and morphological properties of the mesoC material were examined by nitrogen physisorption and electron microscopy investigations, respectively (**Figure 1**). The nitrogen physisorption isotherm of the mesoC presents a distinct type IV shape with a sharp H1-type hysteresis loop, which indicates the presence of a prominent mesoporosity in the carbon material (Figure 1a). Furthermore, a type I isotherm at $p/p_0 \leq 0.1$ is identified, revealing the presence of a small amount of micropores, probably embedded in the carbon wall of the mesoC. The calculated Brunauer–Emmett–Teller (BET) surface area and the total pore volume are 843 $m^2\ g^{-1}$ and 2.90 $cm^3\ g^{-1}$, respectively. Furthermore, the pore size distribution calculated by the quenched solid density functional theory (QSDFT) model shows two narrow maxima positioned at ≈0.76 and ≈12 nm (Figure S1, Supporting Information). This mesopore size value is highly consistent with the average diameter size of the colloidal silica particles used as hard template. The scanning electron microscopy (SEM) image of the mesoC sample in Figure 1b clearly shows a homogeneous and highly porous structure morphology. Furthermore, the high-magnification transmission electron microscopy (TEM) image of the mesoC (Figure 1c) confirms a network with spherical pores inherited from the silica template. Both the shape and pore size of the final mesoC material demonstrate that the resorcinol-formaldehyde polymer used as carbon precursor possesses

© 2015 WILEY-VCH Verlag GmbH & Co. KGaA, Weinheim

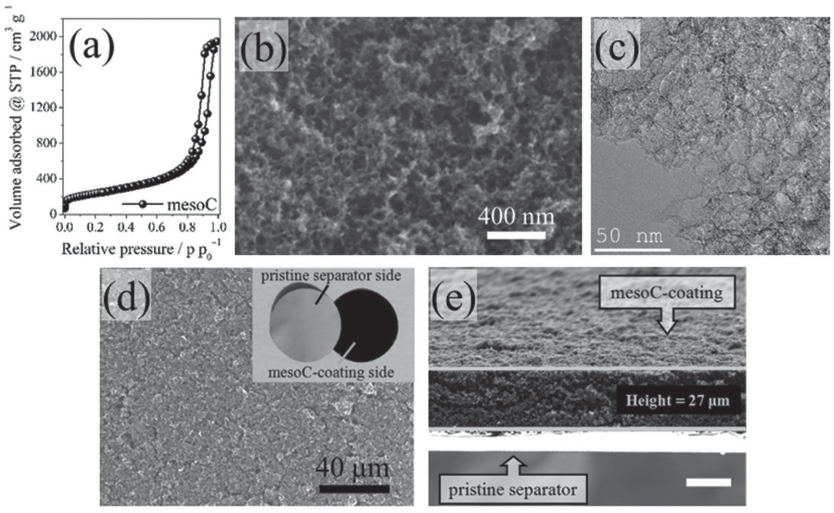

Figure 1. a) Nitrogen physisorption isotherm, b) high-magnification SEM, and c) TEM image of mesoC powder. d) Low-magnification surface SEM image of the mesoC coating. The digital image (inset) shows both sides of the mesoC-coated separator. e) Cross-sectional SEM image of the mesoC-coated separator. Scale bar: 20 µm.

excellent stability at high temperature and good structural replication induced by the silica template. The high surface area and the mesoporous network of the mesoC are crucial for trapping dissolved LiPS species into the mesoC-coating layer and for the further accommodation of the sulfur volume change. For the fabrication of the mesoC-coated separator, a carbon slurry (85 wt% mesoC, 5 wt% conductive super P Li carbon and 10 wt% poly(vinylidene difluoride-*co*-hexafluoropropylene binder (PVDF-HFP)[10] dispersed in *N* -methyl-2-pyrrolidone (NMP) by shaker milling for 1 h) was coated on one side of the pristine separator using the doctor blade technique. As shown in Figure 1d and its corresponding inset, the formed mesoC coating exhibits a dense layer of uniformly distributed carbon particles with no evidences of fissures on the surface. Furthermore, we emphasize the convenient handling of the modified separator owing to the stable adhesion of the carbon slurry to the separator surface and the good flexibility of the designed mesoC-coated separator (Figure S2, Supporting Information). The thickness of the mesoC coating is ≈27 µm (Figure 1e) and due to the low weight of the pristine mesoC, the coating only adds an areal mass loading of 0.5 mg cm^{-2} to the separator, which corresponds to the half weight of the pristine separator.

To examine the stability and textural morphology of the mesoC coating after several discharge–charge cycles, the mesoC-coated separator was inserted between a lithium metal anode and a sulfur cathode, with the mesoC coating facing to the cathode side. The Li–S cell with the mesoC-coated separator was disassembled in a glovebox (after 100 discharge–charge cycles and stopped in the charged state) and the modified separator was thoroughly washed with dioxolane solvent and then dried under vacuum for further ex situ analysis. As shown in **Figure 2**a, the surface SEM image of the cycled mesoC coating reveals the formation of some cracks on the surface of the carbon coating, probably due to the extensive fatigue cycling process of the cell. However, there are no indications for critical damages of the mesoC coating or the network structure. Furthermore, the corresponding energy-dispersive X-ray spectroscopy (EDXS) mapping shows both carbon and sulfur signals consistently distributed with no evidences for agglomerated sulfur-related species. X-ray photo-electron spectroscopy (XPS) measurements, performed after removing the outermost 20 nm from the top of the cycled mesoC-coating surface by ion sputtering, further indicate the presence of elemental sulfur within the mesoC framework (Figure 2b). The high resolution S 2p spectrum of the cycled mesoC coating exhibits three S 2p doublets centered at 162.3, 163.9, and 168.1 eV. The two S 2p doublets located at higher binding energy are assigned to elemental sulfur and to sulfate compounds originating from the lithium bis(trifluoromethanesulfonyl)imide (LiTFSI) electrolyte salt, as it was confirmed by the XP spectra of the fresh sulfur cathode and the LiTFSI-impregnated mesoC-coated separator used as references (Figure S3, Supporting Information). The S 2p doublet positioned at lower binding energy is assigned to terminal sulfur species, indicating that long-chain polysulfide compounds are present within the mesoC-coating matrix. These results clearly demonstrate that the mesoC network of the modified separator limits the LiPS shuttling by trapping/retaining sulfur-related

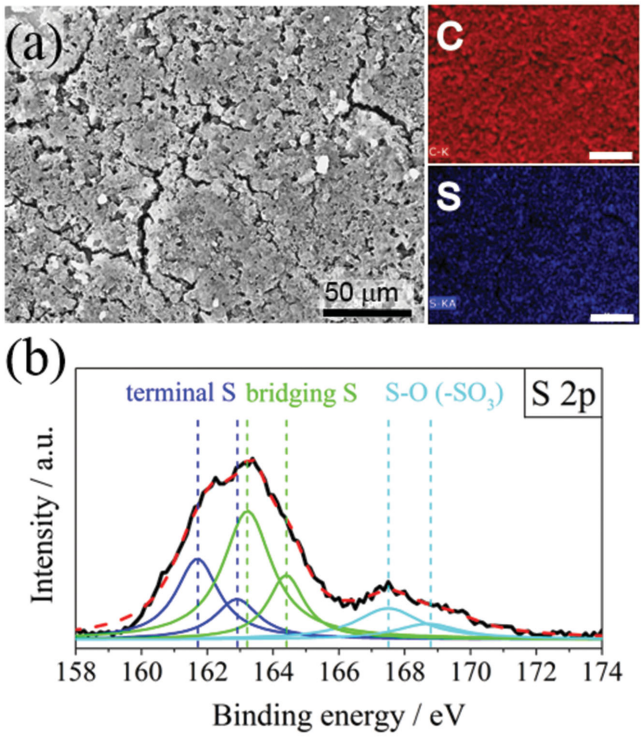

Figure 2. a) SEM image and corresponding EDXS elemental mapping of the cycled mesoC-coated separator. b) High-resolution S 2p XP spectra of the cycled mesoC-coated separator. The black line and the red dashed line correspond to the experimental data and the overall fitted data, respectively.

© 2015 WILEY-VCH Verlag GmbH & Co. KGaA, Weinheim

species, resulting in an improvement of the active material utilization. Furthermore, the use of the mesoC-coated separator also shows lithium-surface-protecting benefits against corrosion, even in the absence of lithium nitrate ($LiNO_3$) additive (Figure S4, Supporting Information).

In order to demonstrate the effectiveness of the mesoC-coated separator on the performance of Li–S batteries, a simple pure sulfur–carbon black cathode was prepared by ball-mixing elemental sulfur, carbon black, and PVDF-HFP (70:20:10 wt%) in NMP. The resulting sulfur cathode contains an areal sulfur loading of ≈1.55 mg cm^{-2}. For comparison, Li–S cells with a pristine separator were tested using a pure sulfur cathode with 50 wt% of sulfur, which corresponds to the sulfur ratio in the cathode when the mass of the mesoC coating is accounted into the 70 wt% sulfur cathode. The internal resistance of fresh Li–S cells was evaluated by electrochemical impedance spectroscopy (EIS) measurements (Figure S5, Supporting Information). The Nyquist plots for the cells with the pristine and the mesoC-coated separator display a single semicircle in the high-to-medium frequency region and an inclined line at low frequency, which are associated to the charge transfer resistance (R_{CT}) and the mass transfer processes, respectively.[11] The R_{CT} value of the Li–S cell with mesoC-coated separator (48 Ω) is approximately two times lower than that of the Li–S cell with pristine separator (110 Ω). The effective decrease of R_{CT} is attributed to the high-electrical conductivity of the mesoC coating which acts in principle as a second current collector, lowering the internal resistance of the cell.[8e] **Figure 3**a,b shows the galvanostatic discharge–charge voltage profiles during the initial ten cycles at a C rate of 0.2 (295 mA cm^{-2}) for the Li–S cells with pristine and mesoC-coated separator. The voltage profiles of both cells exhibit similar voltage plateaus during the discharge–charge processes, which are associated with the typical two-step sulfur redox reactions. The upper discharge plateau at ≈2.33 V is attributed to the conversion of elemental sulfur (S_8) to long-chain polysulfides (Li_2S_n, $4 < n \leq 8$), while

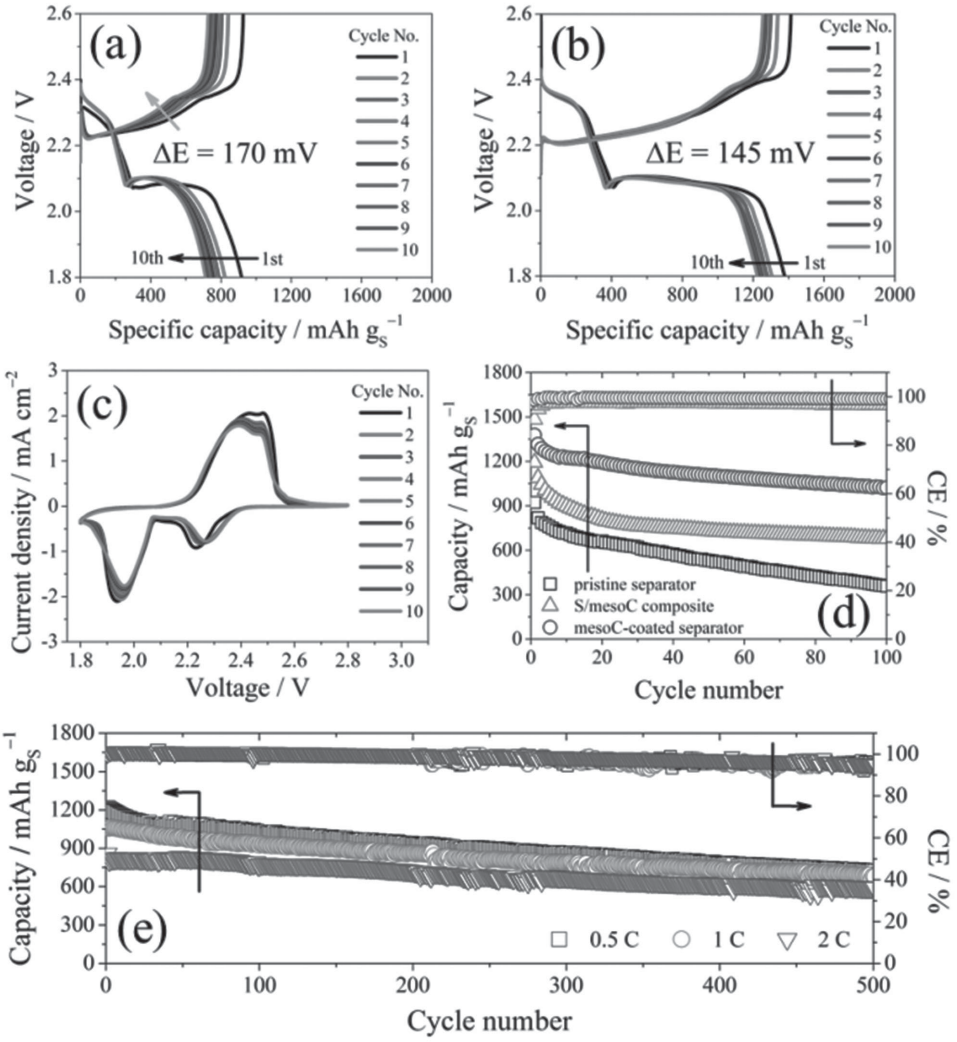

Figure 3. Discharge–charge voltage profiles at 0.2 C of Li–S cells with a) pristine and b) mesoC-coated separator. c) Cyclic voltammograms at a scan rate of 0.1 mV s^{-1} of the Li–S cell with mesoC-coated separator. d) Cycling performance of Li–S cells using a composite cathode, a pristine separator, and a mesoC-coated separator at a current rate of 0.2 C. e) Long-term cycling performance of Li–S cells with mesoC-coated separator at 0.5, 1, and 2 C. The areal sulfur loading of the simple cathodes was ≈1.55 mg cm^{-2}.

© 2015 WILEY-VCH Verlag GmbH & Co. KGaA, Weinheim

the lower discharge plateau at ≈2.10 V corresponds to the formation of the disulfide or monosulfide (Li_2S_2/Li_2S). On the other hand, the charge curves present two continuous plateaus at ≈2.25 and ≈2.36 V, which are related to reversible oxidation reactions of Li_2S_2/Li_2S to S_8/Li_2S_8. However, despite the fact that both Li–S cell types have similar carbon content, there are clear differences in the voltage hysteresis and principally in the length of the voltage plateaus, which are related to redox reaction kinetics and to the reversibility of the system.[9f] The Li–S cell with the mesoC-coated separator shows longer voltage plateaus and lower polarization (ΔE) compared to the Li–S cell with pristine separator. Furthermore, the charge potential increases with the number of cycles for the cell with pristine separator (Figure 3a, highlighted with a gray arrow), while the discharge/charge potentials for the cell with mesoC-coated separator remain almost constant (Figure S6, Supporting Information). A similar trend is observed for both cells when ΔE is analyzed at different current densities (Figure S7, Supporting Information). It is worth mentioning that even under current densities of 5 C, the cells with a mesoC-coated separator still reach discharge capacities of 560 mAh g^{-1} (Figure S7b, Supporting Information). These results clearly demonstrate that the modification of the pristine separator with an electrically conductive mesoC coating is highly beneficial for improving the redox reaction kinetics and the reversibility of the system. Figure 3c shows the cyclic voltammetry (CV) curves of the cell with mesoC-coated separator for the initial ten cycles obtained at a scan rate of 0.1 mV s^{-1}. In the CV curves, two cathodic peaks and two overlapping anodic peaks appear at potentials consistent with those obtained from the discharge–charge voltage profiles discussed above (Figure 3b). From the second cycle, the peak current and the integrated area of the cathodic/anodic peaks are well retained, indicating good cycling reversibility. We compared our advanced cell setup to two commonly used setups to verify the cycling performance of our cell system. Note that the overall cell composition is equal and the cells just differ in their components: i) our advanced cell setup consist of simple mixed carbon black/sulfur cathode and mesoC-coated separator; ii) simple mixed carbon black/sulfur cathode with pristine separator, and iii) mesoC-sulfur composite cathode with pristine separator. The cycling performances conducted at a current rate of 0.2 C for the above-mentioned cells are shown in Figure 3d. The cell with mesoC-coated separator shows an initial discharge capacity of 1378 mAh g^{-1}, which corresponds to 82% of the theoretical capacity of sulfur. After 100 cycles, the same cell exhibits a high discharge capacity of 1021 mAh g^{-1} with an excellent CE of 99.1%. It is worth mentioning that owing to the incorporation of the mesoC-coated separator, Li–S cells are able to demonstrate similar electrochemical performance under either the absence or lower concentration of $LiNO_3$ in the electrolyte, which can be greatly beneficial to improve the cycling life of the cells (Figure S8, Supporting Information). In contrast, the Li–S cell with pristine separator delivers an initial discharge capacity of 922 mAh g^{-1}, e.g., roughly two-thirds of the capacity obtained for the Li–S cell composed of the modified separator. Furthermore, the conventional Li–S cell offers a discharge capacity of only 358 mAh g^{-1} after 100 cycles with a CE of 98.2%. Notably, the moderate cycling performance of the conventional cell configuration with a sulfur–mesoC composite cathode, which exhibits an initial capacity of 1193 mAh g^{-1} and a residual capacity after 100 cycles of 678 mAh g^{-1}, emphasizes even more the benefits of utilizing the functional mesoC-coated separator. The remarkable enhancement on the cycling stability and the high capacity achieved by the simple insertion of a mesoC-coated separator in the Li–S cell are ascribed to the effective trapping of dissolved LiPSs within the mesoporous matrix of the electrically conductive mesoC coating, which limits the LiPS shuttling and thus improves the active material utilization. The LiPS-trapping mechanism is explained considering the complex disordered, 3D pore network of the mesoC coating, which forms a highly intricate pathway against the migration of large LiPSs to the anode side. In addition, Xi et al. recently demonstrated that LiPS species are interfacially adsorbed onto the carbon wall of CNTs.[12] Such physical adsorption can also take place on the extensive interface of the large pore volume, mesoC coating, favoring the retention of the active sulfur material on the cathode side. The long-term cycling performance of the Li–S cells with the mesoC-coated separator was tested at current rates of 0.5, 1, and 2 C (740, 1480, and 2960 mA cm^{-2}, respectively), as shown in Figure 3. After 500 cycles, the cells display excellent discharge capacities of 723, 683, and 591 mAh g^{-1} at, respectively, 0.5, 1, and 2 C, despite the use of a simple cathode mixture containing a high sulfur/nonporous carbon ratio of 7:2. Moreover, the cells still reach a high average CE of ≈96% and capacity fadings of only 0.081%, 0.071%, and 0.062% per cycle, at 0.5, 1, and 2 C, respectively. The low capacity fading and long lifespan of the Li–S cells with a mesoC-coated separator are attributed to the unique features of the mesoC coating which i) effectively reduces the impedance of the sulfur cathode, ii) enables fast electron/lithium ion transport through the carbon network, iii) successfully captures and stores the sulfur species and keeps them accessible as active material for further reutilization, and iv) accommodates the large volume change during the sulfur-to-Li_2S reaction. To get information about the coating thickness effect on the cycling performance, we prepared three modified separators with mesoC-coating thickness of 15, 30, and 65 µm. These modified separators were introduced in Li–S cells which use simple sulfur cathodes with a higher areal sulfur loading of 3.5 mg cm^{-2}. A conventional cell composed of a pristine separator and a sulfur cathode with 50 wt% of sulfur and areal loading of ≈3.5 mg cm^{-2} was used for comparison, considered as a high sulfur loading.[13] **Figure 4**a shows the cycling performance of Li–S cells using a pristine separator and mesoC-coated separators with different coating thickness cycled at a current rate of 0.2 C. As we expected, when the coating thickness (with sulfur rate in parentheses) decreases from 65 (48.2%) to 30 (50.7%) and 15 (52.6%) µm, the average capacity decreases with a somewhat linear trend (Figure 4b), indicating probably less affinity to retain the high concentration of LiPSs in the electrolyte. Nevertheless, all the three cells with a modified separator exhibit a stable cycling performance and even the cell with the thinnest coating layer is able to deliver a doubled capacity compared to the conventional cell with lower sulfur content. Latter cell deactivates much faster than the cell with higher sulfur content which cannot be expected at first view. Overall, the electrochemical performance and long cycling life of our Li–S cells with

© 2015 WILEY-VCH Verlag GmbH & Co. KGaA, Weinheim

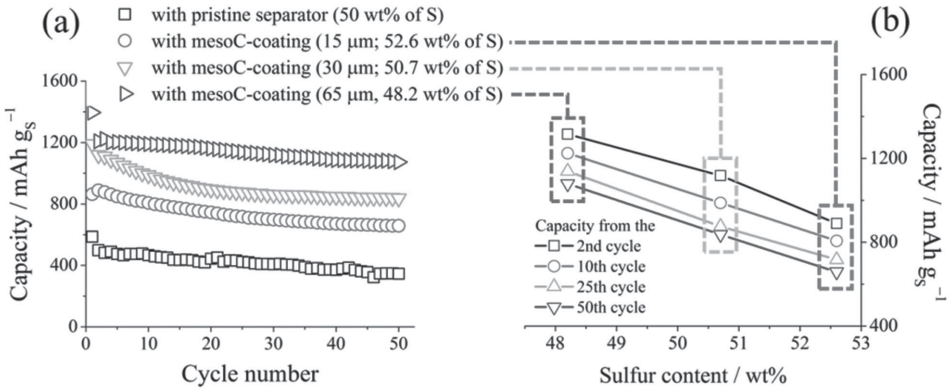

Figure 4. a) Cycling performance of Li–S cells using a pristine separator and mesoC-coated separators with different coating thicknesses. The thickness of the mesoC coating and the sulfur content of the whole cathode region are shown in parentheses. The cells were cycled at a current rate of 0.2 C and the areal sulfur loading of the simple cathode was ≈3.5 mg cm^{-2}. b) Capacity at different cycling numbers versus sulfur content. Data obtained from Figure 4a.

mesoC-coated separator exceeds that of conventional Li–S cells with pristine separator and complex sulfur–carbon composites,[14] and shows an improved performance compared with recently reported Li–S cells using microporous carbon-modified separator designs (Table S1, Supporting Information).[9]

3. Conclusions

We have proposed a mesoporous carbon-coated separator as a functional separator for improving the overall performance of Li–S batteries. Straight-forward modification of a commercial polypropylene separator allowed the integration of a conductive mesoporous carbon layer which offers a physical place to localize dissolved polysulfide intermediates and retain them as active material on the cathodic side to improve its reutilization. As a result, the Li–S batteries with a mesoC-coated separator showed significant performance enhancements: high capacity, long cycle life, and low capacity fading at different current rates. Our results highlight the importance of the rational design of modified separators with mesoporous carbon structures and this proof of concept may bring reliability for advanced high-performance Li–S batteries.

4. Experimental Section

MesoC Fabrication: The mesoC material employed in this paper was prepared by our previously reported polymerization of resorcinol-formaldehyde in the presence of 12 nm in diameter silica hard template, using a silica/resorcinol ratio of 3.[8e] The silica-containing carbon product obtained after carbonization in an argon atmosphere at 900 °C for 2 h was treated with 20% hydrofluoric acid (Aldrich) to etch away the template, washed thoroughly with deionized water, and dried at 100 °C before use it.

MesoC-Coated Separator Preparation: The commercial polypropylene separator (Celgard 2500) was modified by direct coating of a carbon slurry (85 wt% mesoC powder, 5 wt% Super P Li Carbon (BASF) and 10 wt% PVDF-HFP (Solef 21216) in NMP (Aldrich) solution) on one side of the separator using a doctor blade method. Then, the modified separator was dried in an oven at 40 °C for 20 h under air. Finally, the obtained mesoC-coated separator was punched into circular disks for assembling cells.

Simple Sulfur and Conventional Composite Cathodes Fabrication: Both the simple mixed sulfur–carbon black cathode and the sulfur–mesoC composite cathode were prepared by shaker-milling commercial elemental sulfur (Aldrich) or sulfur–mesoC composite (containing ≈70 wt% of sulfur after melt-infiltration at 155 °C for 5 h in Ar atmosphere, Figure S9, Supporting Information), Super P Li Carbon and PVDF-HFP (70:20:10 wt%) in NMP. The obtained viscous slurry was coated onto an aluminum foil current collector by doctor blade method and dried at 50 °C for 20 h in an air oven. Finally, the sulfur cathodes were cut into circular disks of 12 mm. Depending on the electrochemical test, the areal sulfur loading of the sulfur cathodes was 1.55 or 3.5 mg cm^{-2}. For comparison, conventional Li–S cells with pristine separator and simple sulfur cathode were tested using a cathode with 50 wt% of sulfur.

Preparation of Li–S Cells: CR2025-type stainless steel coin cells were assembled in an Ar-filled glove box. The electrolyte solution was 1 M LiTFSI salt (BASF, dried at 100 °C in vacuum overnight) in a mixed solvent of 1,3-dioxolane (DOL, Aldrich) and 1,2-dimethoxyethane (Aldrich) (1:1 by volume), with 0.25 M $LiNO_3$ (Merck) as additive. Despite the incorporation of the mesoC coating is able to moderate the corrosion/contamination effect of the lithium surface from side reactions between metallic lithium and dissolved polysulfides, even in the absence of $LiNO_3$, $LiNO_3$ was added to ensure the protection of the lithium anode from possible electrolyte depletion. Lithium metal foil (ABCR, diameter 13 mm, thickness 250 µm) was used as anode material and reference electrode. A commercial microporous polypropylene separator (Celgard 2500, diameter 16 mm) was used as pristine separator. The mesoC-coated separator was placed between the sulfur cathode and the lithium anode with the carbon coating facing to the cathode side.

Electrochemical Measurements: The cells were cycled at room temperature using a BaSyTec cell test system in a potential window of 1.8–2.6 V at various cycling rates (0.2–4 C), based on the mass and theoretical capacity of sulfur (1 C = 1672 mA g^{-1}). Those cells cycled in the absence of $LiNO_3$ were cycled between 1.5 and 2.8 V. Cyclic voltammetry (CV) tests and EIS measurements were performed using a VMP3 potentiostat (Bio-logic). The cyclic voltammograms were recorded at a scan rate of 0.1 mV s^{-1} with a potential range of 1.8–2.8 V. EIS measurement were recorded from 200 kHz to 100 mHz with an AC voltage amplitude of 5 mV at the open-circuit voltage of the cells. Prior to carry out the long-term cycling tests at 0.5 and 1 C rates, the cells were cycled at 0.2 C for the first two cycles as forming process.

Characterization: SEM images were taken with a Gemini 1530 mixroscope (LEO) at 15–20 kV acceleration voltage. EDXS measurements were taken on the SEM with an EDXS spectrometer from Bruker. TEM measurements were carried out with a Philips CM20 microscope equipped with a field emission gun working at 200 kV

© 2015 WILEY-VCH Verlag GmbH & Co. KGaA, Weinheim

acceleration voltage. Nitrogen sorption experiments were realized using a Quantachrome Quadrasorb SI instrument and data analysis was performed using the Quantachrome Quadrawin 4.0 software. Prior to the measurement, the sample was degassed under dynamic vacuum at 150 °C for 24 h. Specific surface area was calculated at a relative pressure of 0.05–0.2, using the multipoint BET method. The total pore volume was determined at $p\ p_0^{-1} = 0.97$. The pore size distribution was obtained using the QSDFT equilibrium model. XPS measurements were carried using a PHI 5600 spectrometer (Physical Electronics) equipped with a hemispherical analyzer operated at pass energy of 29 eV. Monochromated Al Kα radiation (350 W, λ = 1486.7 eV) was used applying partly low energy electrons for charge compensation. To avoid any contact of the samples with air, a sealed container was used to transfer the samples from the Ar-filled glovebox into the vacuum chamber of the XP spectrometer. In order to examine the subsurface part of the mesoC coating, sputtering was performed using Ar^+ ions at 3.5 keV for 10 min (sputter rate: 3.5 nm min^{-1} at SiO_2). A similar procedure was performed for the fresh sulfur cathode and the Li-TFSI-impregnated mesoC-coated separator, which were used as references. All spectra were calibrated using the C 1s level (284.8 eV) as reference. The cycled mesoC-coated separators were washed with DOL solvent inside the glove box prior to the SEM/EDXS and XPS investigations.

Supporting Information

Supporting Information is available from the Wiley Online Library or from the author.

Acknowledgements

The authors thank Andrea Voß, Anne Voidel, and Ronny Buckan for their valuable technical support and Cornelia Geringswald for thermogravimetric analysis. The authors gratefully acknowledge financial support from the German Federal Ministry of Education and Research (BMBF) through the Excellent Battery-WING Center "Batteries-Mobility in Saxony" (Grant Nos. 03X4637B and 03X4637C).

Received: June 2, 2015
Published online: July 24, 2015

[1] a) P. G. Bruce, B. Scrosati, J.-M. Tarascon, *Angew. Chem. Int. Ed.* **2008**, *47*, 2930; b) V. Etacheri, R. Marom, R. Elazari, G. Salitra, D. Aurbach, *Energy Environ. Sci.* **2011**, *4*, 3243.

[2] a) A. Manthiram, Y. Fu, S.-H. Chung, C. Zu, Y.-S. Su, *Chem. Rev.* **2014**, *114*, 11751; b) Z. Lin, C. Liang, *J. Mater. Chem. A* **2015**, *3*, 936.

[3] Y. V. Mikhaylik, J. R. Akridge, *J. Electrochem. Soc.* **2004**, *151*, A1969.

[4] a) J. Wang, Z. Yao, C. W. Monroe, J. Yang, Y. Nuli, *Adv. Funct. Mater.* **2013**, *23*, 1194; b) J.-W. Park, K. Ueno, N. Tachikawa, K. Dokko, M. Watanabe, *J. Phys. Chem. C* **2013**, *117*, 20531; c) Z. W. Seh, W. Li, J. J. Cha, G. Zheng, Y. Yang, M. T. McDowell, P.-C. Hsu, Y. Cui, *Nat. Commun.* **2013**, *4*, 1331; d) G. Zhou, Y. Zhao, C. Zu, A. Manthiram, *Nano Energy* **2015**, *12*, 240; e) L. Xiao, Y. Cao, J. Xiao, B. Schwenzer, M. H. Engelhard, L. V. Saraf, Z. Nie, G. J. Exarhos, J. Liu, *Adv. Mater.* **2012**, *24*, 1176; f) F. Wu, J. Chen, R. Chen, S. Wu, L. Li, S. Chen, T. Zhao, *J. Phys. Chem. C* **2011**, *115*, 6057; g) I. Bauer, S. Thieme, J. Brückner, H. Althues, S. Kaskel, *J. Power Sources* **2014**, *251*, 417.

[5] a) X. Ji, K. T. Lee, L. F. Nazar, *Nat. Mater.* **2009**, *8*, 500; b) N. Jayaprakash, J. Shen, S. S. Moganty, A. Corona, L. A. Archer, *Angew. Chem. Int. Ed.* **2011**, *50*, 5904; c) C. Zhang, H. B. Wu, C. Yuan, Z. Guo, X. W. Lou, *Angew. Chem. Int. Ed.* **2012**, *51*, 9592; d) M. Klose, K. Pinkert, M. Zier, M. Uhlemann, F. Wolke, T. Jaumann, P. Jehnichen, D. Wadewitz, S. Oswald, J. Eckert, L. Giebeler, *Carbon* **2014**, *79*, 302; e) C. Hoffmann, S. Thieme, J. Brückner, M. Oschatz, T. Biemelt, G. Mondin, H. Althues, S. Kaskel, *ACS Nano* **2014**, *8*, 12130; f) N. Ding, Y. Lum, S. Chen, S. W. Chien, T. S. A. Hor, Z. Liu, Y. Zong, *J. Mater. Chem. A* **2015**, *3*, 1853.

[6] a) L. Ma, H. Zhuang, Y. Lu, S. S. Moganty, R. G. Hennig, L. A. Archer, *Adv. Energy Mater.* **2014**, *4*, 1400390; b) G. Ma, Z. Wen, Q. Wang, C. Shen, J. Jin, X. Wu, *J. Mater. Chem. A* **2014**, *2*, 19355.

[7] a) J. Hassoun, B. Scrosati, *Angew. Chem. Int. Ed.* **2010**, *49*, 2371; b) J. Brückner, S. Thieme, F. Böttger-Hiller, I. Bauer, H. T. Grossmann, P. Strubel, H. Althues, S. Spange, S. Kaskel, *Adv. Funct. Mater.* **2014**, *24*, 1284; c) T. Jaumann, M. Herklotz, M. Klose, K. Pinkert, S. Oswald, J. Eckert, L. Giebeler, *Chem. Mater.* **2015**, *27*, 37; d) C. Zu, M. Klein, A. Manthiram, *J. Phys. Chem. Lett.* **2014**, *5*, 3986.

[8] a) Y.-S. Su, A. Manthiram, *Nat. Commun.* **2012**, *3*, 1166; b) Y.-S. Su, A. Manthiram, *Chem. Commun.* **2012**, *48*, 8817; c) X. Wang, Z. Wang, L. Chen, *J. Power Sources* **2013**, *242*, 65; d) R. Singhal, S.-H. Chung, A. Manthiram, V. Kalra, *J. Mater. Chem. A* **2015**, *3*, 4530; e) J. Balach, T. Jaumann, M. Klose, S. Oswald, J. Eckert, L. Giebeler, *J. Phys. Chem. C* **2015**, *119*, 4580.

[9] a) S.-H. Chung, A. Manthiram, *J. Phys. Chem. Lett.* **2014**, *5*, 1978; b) S.-H. Chung, A. Manthiram, *Adv. Funct. Mater.* **2014**, *24*, 5299; c) S.-H. Chung, A. Manthiram, *Adv. Mater.* **2014**, *26*, 7352; d) H. Wei, J. Ma, B. Li, Y. Zuo, D. Xia, *ACS Appl. Mater. Interfaces.* **2014**, *6*, 20276; e) H. Yao, K. Yan, W. Li, G. Zheng, D. Kong, Z. W. Seh, V. K. Narasimhan, Z. Liang, Y. Cui, *Energy Environ. Sci.* **2014**, *7*, 3381; f) G. Zhou, S. Pei, L. Li, D.-W. Wang, S. Wang, K. Huang, L.-C. Yin, F. Li, H.-M. Cheng, *Adv. Mater.* **2014**, *26*, 625.

[10] M. J. Lacey, F. Jeschull, K. Edström, D. Brandell, *J. Phys. Chem. C* **2014**, *118*, 25890.

[11] M. V. Reddy, T. Yu, C. H. Sow, Z. X. Shen, C. T. Lim, G. V. Subba Rao, B. V. R. Chowdari, *Adv. Funct. Mater.* **2007**, *17*, 2792.

[12] K. Xi, B. Chen, H. Li, R. Xie, C. Gao, C. Zhang, R. V. Kumar, J. Robertson, *Nano Energy* **2015**, *12*, 538.

[13] P. Strubel, S. Thieme, T. Biemelt, A. Helmer, M. Oschatz, J. Brückner, H. Althues, S. Kaskel, *Adv. Funct. Mater.* **2015**, *25*, 287.

[14] a) C. Nan, Z. Lin, H.-G. Liao, M.-K. Song, Y. Li, E. J. Cairns, *J. Am. Chem. Soc.* **2014**, *136*, 4659; b) C. Xu, Y. Wu, X. Zhao, X. Wang, G. Du, J. Zhang, J. Tu, *J. Power Sources* **2015**, *275*, 22.

© 2015 WILEY-VCH Verlag GmbH & Co. KGaA, Weinheim